NATIONAL ENERGY TECHNOLOGY LABORATORY

# GRANULAR TEMPERATURE MODELING WITH LARGE-SCALE CFD-DEM DATA

Aug. 28th, **2024**

**DOE/NETL-2024/4482**

U.S. DEPARTMENT OF ENERGY | NATIONAL ENERGY TECHNOLOGY LABORATORY

# DISCLAIMER

This project was funded by the National Nuclear Security Administration (NNSA), through the Minority Serving Institutions Internship Program (MSIIP) at the National Energy Technology Laboratory an agency of the United States Government, through an appointment administered by the Oak Ridge Institute for Science and Education. 

# Granular temperature modeling with large-scale CFD-DEM data

Manan Raval[1] and William D. Fullmer[2]
[1]*New Jersey Institute of Technology, Newark, NJ 07102*
[2]*National Energy Technology Laboratory, Morgantown WV 26505*

## 1. INTRODUCTION

When particles are fluidized by a gas, the resulting multiphase flow is almost always complex and chaotic, generating heterogeneous structures commonly known as clusters in particle-dilute flows and bubbles in particle-dense flows (Agrawal, et al. 2001; Fullmer and Hrenya 2018). These heterogeneous structures create a modeling challenge. While methods such as kinetic-theory based two-fluid models (Garzó, et al. 2013) are able to capture these dynamics, it takes a significant amount of resolution to do so (Fullmer and Hrenya 2016, Fullmer, et al. 2017). Coarse-grid approaches targeting large-scale, industrially-relevant problems are unable to actively resolve the small-scale dynamics. Thus far, modeling has proved challenging with most efforts focused on the filtered (unresolved) drag force, e.g., Igci, et al. (2008), Igci & Sundaresan (2011), Sarkar, et al. (2016), Ozel et al. (2017), among many others. In this work, we focus on another quantity, the granular temperature, $\Theta$, a measure of the fluctuating kinetic energy in the particle phase.

The model data come from a recently conducted large-scale CFD-DEM simulation campaign. In the CFD-DEM method, the particles are resolved individually, including all collisions, and the fluid grid is twice the particle size, $dx = 2d_p$. The problem of interest is gravity driven, particle-laden, gas-solid flow in a triply-periodic domain of length $L_x = 2048$ particle diameters with an aspect ratio of 4, $L_x = L_z = L_y/4$. The mean particle concentration, $\phi_0 = N_p(\pi/6)d_p^3/L_xL_yL_z$ for $N_p$ particles in the domain, and the Archimedes number, $Ar = \rho_g\Delta\rho|\mathbf{g}|d_p^3/\mu_g^2$, are varied over a 33-point phase-space as shown in Fig. 1. Constant properties for all 33 simulations are the particle-to-fluid density ratio, $\rho^* = \rho_p/\rho_g = 1000$, the particle-particle restitution coefficient, $e_{pp} = 0.9$, and the friction coefficient, $\mu_{pp} = 0.25$. The mean (global) particle velocity is constrained to zero. Cluster-induced turbulence generates heterogeneous structures which cause particles to fall in dense clusters and rise in the dilute gas streams as exemplified by some example snapshots in Fig. 1. Once a quasi-steady-state has been reached, a snapshot is saved 100 times for each simulation at a frequency of $\tau_p = \rho_p d_p^2/18\mu_g = 0.025$ s. The CFD-DEM data is post-processed to compute the granular temperature and average over the entire domain. Two methods are used to calculate the granular temperature: 1) grid based, e.g., using the local eight fluid cells surrounding a given particle, and 2) filtered, using a constant diffusion filter width of $\delta_f = 8d_p$.

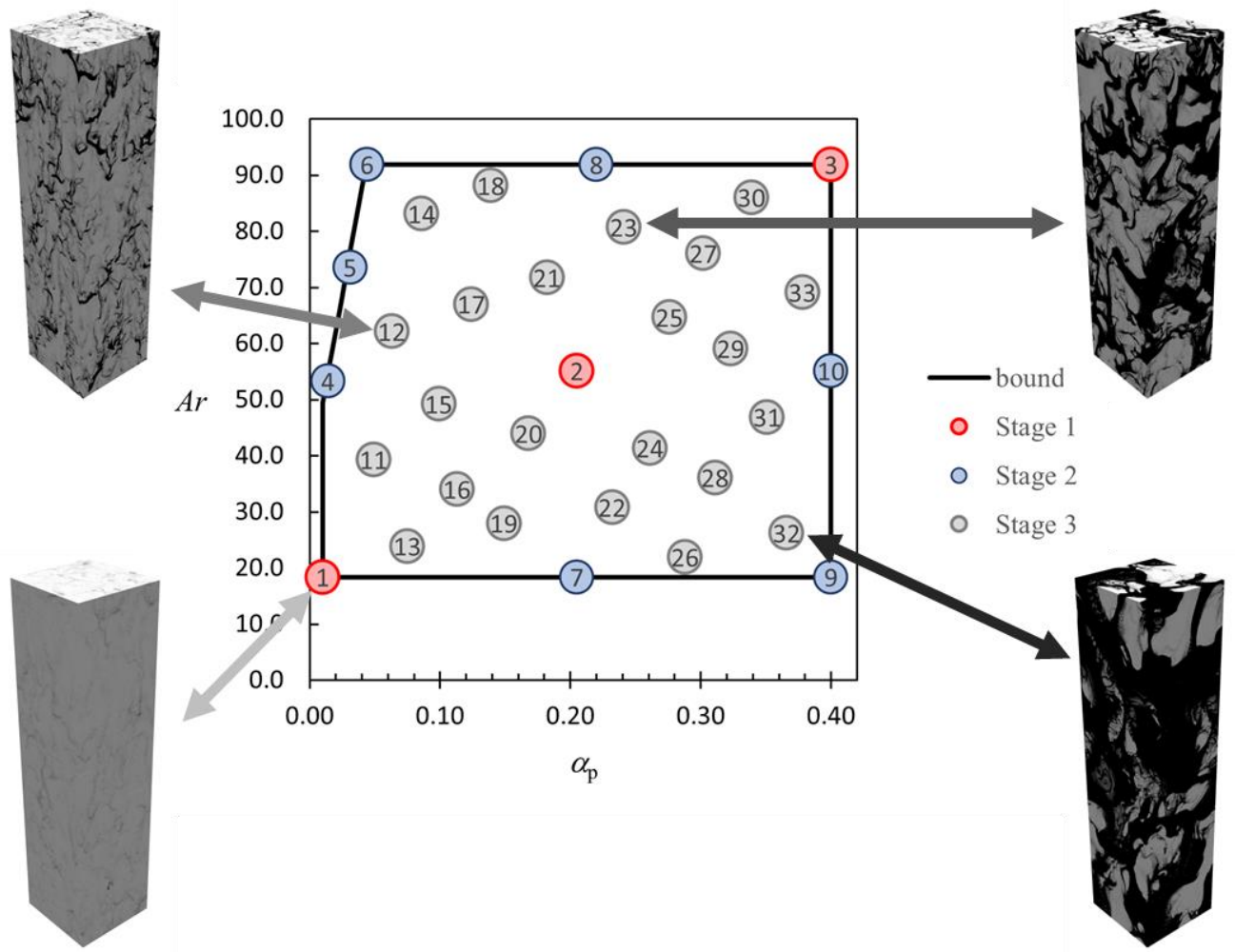


**Fig. 1. Overview of the 33-point phase space in mean concentration and Archimedes number with example snapshots for cases: run-01, run-12, run-23, and run-32.**

## 2. MODEL EQUATIONS

We will rely on two models to estimate the granular temperature in this work. The first results from the homogeneous equilibrium assumption of the kinetic theory of Garzó et al. (2012). This assumption drastically simplifies the model by eliminating all transient and gradient terms, leaving only two algebraic expressions. The first gives the (homogeneous) slip velocity as

$$v_{slip} = |v_p - v_g| = \frac{u_\infty}{F^*} = \frac{\Delta\rho |\boldsymbol{g}| d_p^2}{18\mu_g F^*}, \tag{1}$$

where $u_\infty$ is the terminal velocity (of a single in an infinite medium) and $F^*$ is the multi-particle drag law, i.e., $F^* = C_d/C_{d\infty}$. In this work we use the DNS-based drag model of Tang et al. (2015). This is the same

drag law that was used in the original MFIX-Exa CFD-DEM simulations. The second expression gives the (homogeneous) granular temperature,

$$\xi = \frac{2\gamma}{m}\Theta + \zeta_0\Theta\,, \tag{2}$$

where $\Theta$ is the granular temperature and $m = \rho_p(\pi/6)d_p^3$, is the particle mass. Equation (2) describes the balance of fluctuating kinetic energy generated by the neighbor effect, $\xi$, and dissipated by the gas through thermal drag, $\gamma$, and the particle inelasticity through the zeroth-order cooling rate, $\zeta_0$. The neighbor effect is given by,

$$\xi = \frac{d_p}{3}\left(\frac{3\pi\mu_g d_p}{m}\right)^2 \frac{v_{slip}^2}{\sqrt{\Theta}} S^*\,, \tag{3}$$

where $S^* = S^*(\phi)$ is the concentration dependence of $\xi$. The thermal drag force is given by,

$$\gamma = 3\pi\mu_g d_p R^* \tag{4}$$

where $R^* = R_0^*(\phi) + R_1^*(\phi)Re_\Theta$ is the concentration dependence of $\gamma$, which also includes a first order dependence on the thermal Reynolds number,

$$Re_\Theta = \frac{\rho_g\sqrt{\Theta}d_p}{\mu_g}\,.$$

Finally, the zeroth-order cooling rate is given by

$$\zeta_0 = \frac{8}{d_p}\phi\chi\left(1 - e_{pp}^2\right)\left(1 + \frac{3}{16}a_2\right)\sqrt{\frac{\Theta}{\pi}}, \tag{5}$$

where $a_2$ is the kurtosis of the velocity distribution function, see Garzó et al. (2012). The concentration dependent functions S*, $R_0^*$, and $R_1^*$ are all fit to DNS data as with drag, $F^*$; see Fullmer et al. (2017) for the exact expressions used in this work.

The second model used here is the simple expression of Tang et al. (2016),

$$Re_\Theta = 2.108\frac{Re_p^{0.85}}{\sqrt{\rho^*}}\,, \tag{5}$$

where $Re_\Theta$ is the thermal Reynolds number as before and $Re_p$ is the particle (mean flow) Reynolds number,

$$Re_p = \frac{\rho_g(1-\phi)v_{slip}d_p}{\mu_g}\,.$$

Equation (5) was fit to DNS data of dynamic suspensions. Therefore it is not necessarily as restrictive as the homogeneous equilibrium assumption on the kinetic theory, but the DNS simulations were much, much smaller than the CFD-DEM simulation data that is considered here.

# 3. RESULTS

As mentioned previously, there are two post-processed datasets, one without filtering and one with Gaussian filtering of width $\delta f = 8d_p$. The same analysis will be applied to both datasets individually, revealing some interesting similarities and differences. We begin the analysis by looking at run-02 which is the center-point of the phase-space, see Fig. 1. First, we show the phase-averaged granular temperature as a function of time in Fig. 2. Note that this granular temperature quantity is both phase-averaged and spatially averaged over the entire domain, i.e.,

$$\langle\langle\Theta\rangle\rangle = \frac{\langle\phi\Theta\rangle}{\langle\phi\rangle} = \frac{\iiint \phi\Theta \, dx \, dy \, dz}{\iiint \phi \, dx \, dy \, dz}. \tag{7}$$

Note that $\langle\phi\rangle \approx \phi_0$ but minor differences exist due to the numerical process of depositing particle properties onto the grid and then averaging the Eulerian quantity. The fluctuation of the granular temperature in run-02 for both the filtered and no-filtered method are virtually identical, however the magnitude in the filtered data is much higher compared to the non-filtered data. This is somewhat expected due to the larger volume used to compute the granular temperature, i.e., more particles are included in the averaging, increasing the likelihood of averaging particles with different velocity.

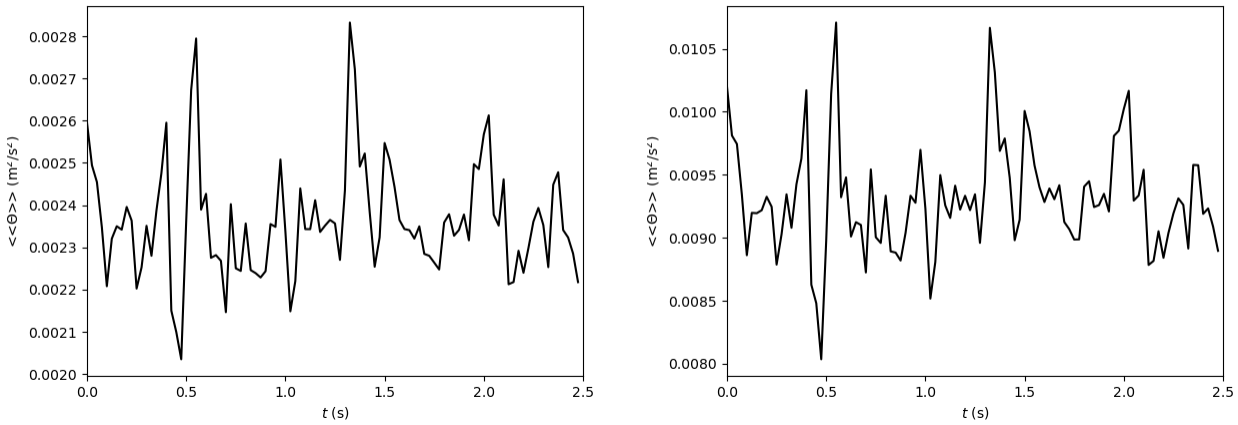


**Fig. 2. Phase- and space-averaged granular temperature as a function of time for run-02, no filtering on the left and filtered, $\delta f = 8d_p$, on the right. Note that the data output frequency is one $\tau_p = 0.025$ s resulting in the noisy expected signal which is, ideally, statistically independent of the previous (saved) time.**

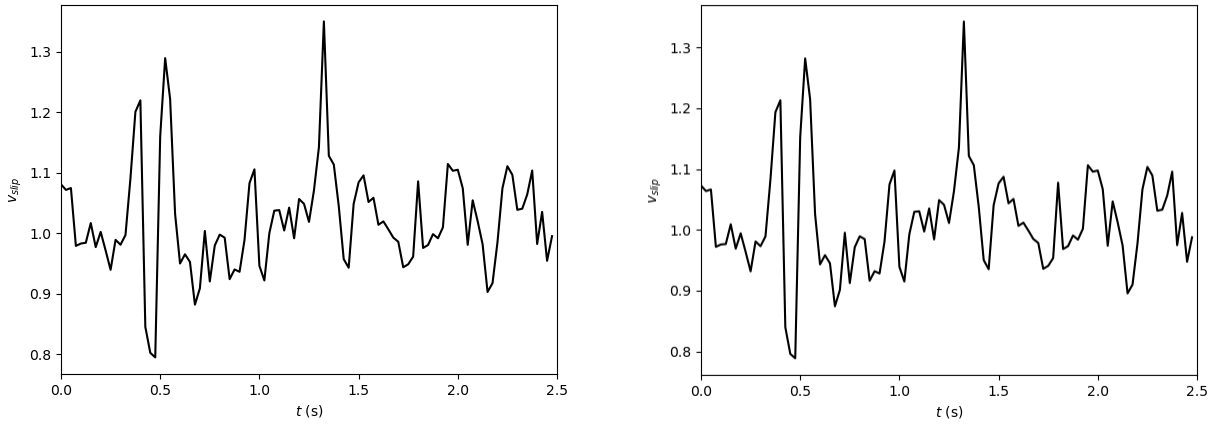


**Fig. 3. Mean slip velocity as a function of time for run-02, no filtering on the left and filtered, $\delta f = 8d_p$, on the right.**

Another important parameter is the slip velocity,

$$v_{slip} = \left| \langle\langle v_p \rangle\rangle - \langle\langle v_g \rangle\rangle \right| . \tag{8}$$

In these simulations, the global average particle velocity is constrained to be zero in all directions, i.e., $\langle v_p \rangle = 0$, therefore $\langle\langle v_p \rangle\rangle = 0$, and $v_{slip}$ is simply $|\langle\langle v_g \rangle\rangle|$. The slip velocity for the non-filtered and filtered data of run-02 is shown in Fig 3. Like the granular temperature in Fig. 2, the slip velocity with and without filtering are strongly correlated. However, unlike the granular temperature, there is not a noticeable difference in magnitude. In fact, the slip velocity is virtually unaffected by filtering. For reference, the homogeneous slip velocity in this case is $v_{slip}^{(H)} = 0.135$ m/s given by the drag law of Tang et al. (2016) which was also used in the underlying CFD-DEM simulations. The phase-averaged slip velocity is nearly an order of magnitude larger than the homogeneous value. This is not surprising given the highly heterogeneous and dynamic CIT state, e.g., as typified in Fig. 1.

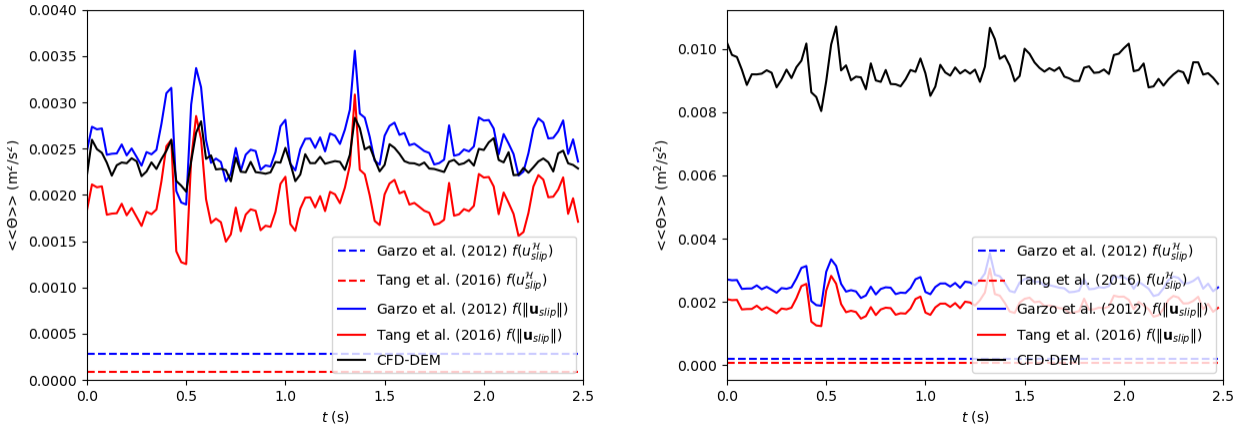


**Fig. 4. Granular temperature as a function of time for run-02, no filtering on the left and filtered, $\delta f = 8d_p$, on the right, compared to the models of Garzó et. al. (2012) (blue) and Tang et al. (2016) (red) using the homogeneous slip velocity (dashed lines) and the actual, measured slip velocity (solid lines).**

Now, we compare the average granular temperature data from our CFD-DEM simulation campaign to homogeneous predictions, specifically the homogeneous equilibrium state of the kinetic theory of Garzó et al. (2012), Eq. (2), and the simple correlation given by Tang et al. (2016), Eq. (5). In Fig. 4, these predictions are compared to the phase-averaged granular temperature of run-02 (previously shown in Fig. 2) As with the slip velocity, the predictions of these models are very far from the granular temperature extracted from the CFD-DEM simulations. And, again, this is not surprising, but provides a baseline and framework for exploring more complex modeling approaches. Next, we simply attempt to use these same models replacing the (homogeneous) slip velocity with the calculated slip velocity, i.e., from the simulation results as given in Fig. 3. Figure 4 also shows that using the actual slip velocity now allows both models to predict the average granular temperature quite well for the case of unfiltered data. We see that the model of Garzó et al. (2012) slightly overestimates the CFD-DEM data while the model of Tang et al. (2016) slightly underestimates the data. On the other hand, when this approach is applied to the filtered data, the measured granular temperature is still significantly higher than the modified predictions.

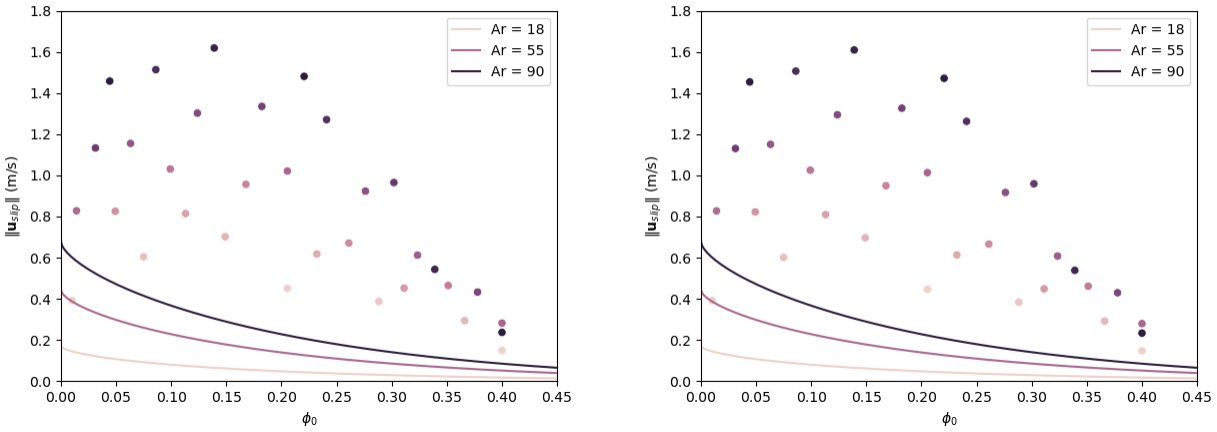


**Fig. 5. Time-averaged mean slip velocity as a function of the global particle concentration, no filtering on the left and filtered, $\delta f = 8d_p$, on the right.**

After looking at only run-02 data, we now consider all the runs for both the unfiltered and filtered simulation data. To reduce the data, we calculated the time-averaged granular temperature and the average slip velocity for each run. The time- and domain-averaged mean slip velocity is shown as points in Fig. 5. The homogeneous slip velocity is given by the family of curves which depend on the Archimedes number with minimum, mean, and maximum values shown. The data points are colored by the scale of *Ar* which coincides with the homogeneous slip velocity curves. We see that the higher *Ar* values typically correspond to a higher the slip velocity, indicating a larger degree of clustering or heterogeneity. The general behavior, i.e., increasing slip velocity to with concentration to approximately 10 to 15% and then decaying asymptotically to the homogeneous value at high concentration ($\phi_0 > 40\%$), has been observed previously in similar studies, e.g., Radl and Sundaresan (2015) and Fullmer and Hrenya (2016). As with run-02 in Fig. 3, there is no significant difference between the unfiltered and filtered data for the slip velocity.

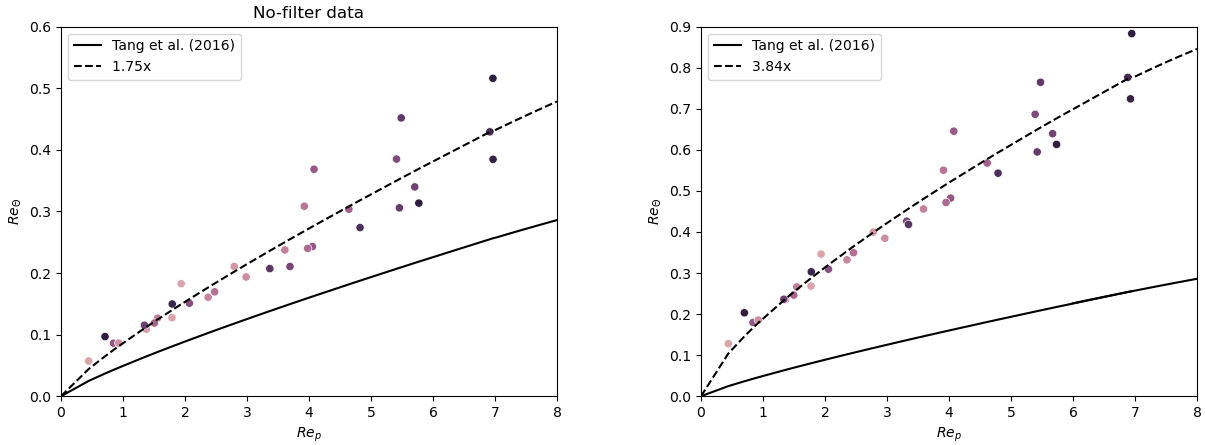


**Fig. 6. Time- and phase-averaged granular temperature re-fit using the model of Tang et al. (2016), no filtering on the left and filtered, $\delta f = 8d_p$, on the right.**

Next, we consider the time-averaged granular temperature for the full 33-point dataset. The data is again color coded by *Ar* using the same scale as in Fig. 5. At this point, both the Garzó et al. (2012) and the Tang et al. (2015) were shown to provide a good estimate of granular temperature—provided that the *actual* slip velocity is used—for the unfiltered data and both under-predicted the filtered data. Therefore, for the rest of this work we will only consider the model of Tang et al (2016) which is considerably simpler and easier to adjust because it is a data-fit correlation. Figure 6 shows the time-averaged granular temperature for all simulations. For unfiltered data, the model of Tang et al. (2016) compares very favorably with the data, appearing only to need a slight increase in the coefficient to fit the data. While this is indeed the case, we have also freed the exponential parameter and preformed a two-parameter best-fit using Python's library, scikit-learn. The result is a leading coefficient 1.75-times larger and an exponent of 0.83, very close to the value of 0.85 suggested by Tang et al. (2016). Although we are using the heterogeneous slip velocity, this still seems to be an impressive result considering that the original model was fit on DNS data of no more than 500 particles. The filtered data requires slightly more adjustment, a leading coefficient 3.84-times as large and a slightly smaller exponent of 0.73. To summarize, the adjusted fits are,

$$Re_\Theta = 3.689 \frac{Re_p^{0.83}}{\sqrt{\rho^*}}, \tag{9}$$

for the unfiltered data, and

$$Re_\Theta = 8.095 \frac{Re_p^{0.73}}{\sqrt{\rho^*}}, \tag{10}$$

for the filtered data.

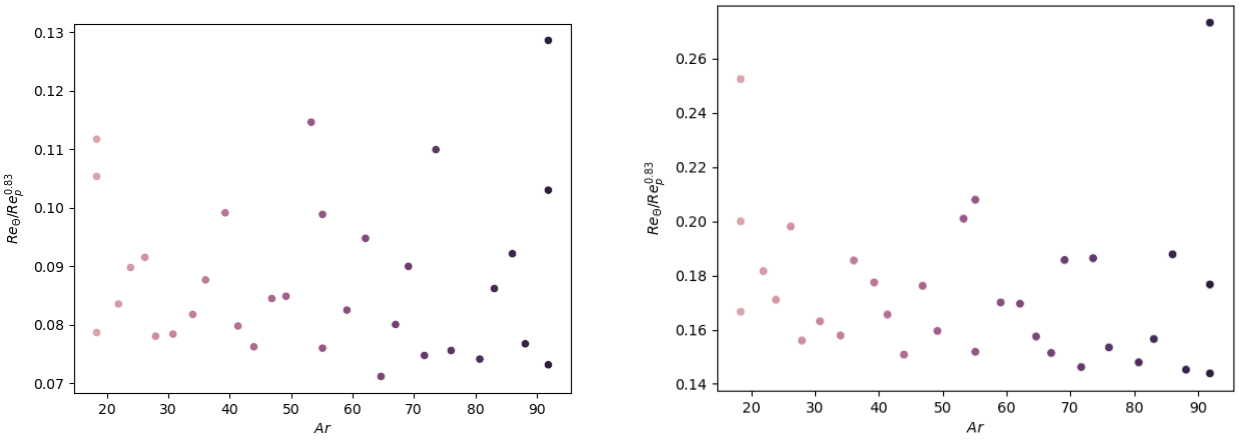


**Fig. 7. Ratio of $Re_\Theta$ to the primary influence of the adjusted Tang fit as a function of *Ar*, no filtering on the left and filtered, $\delta f = 8d_p$, on the right.**

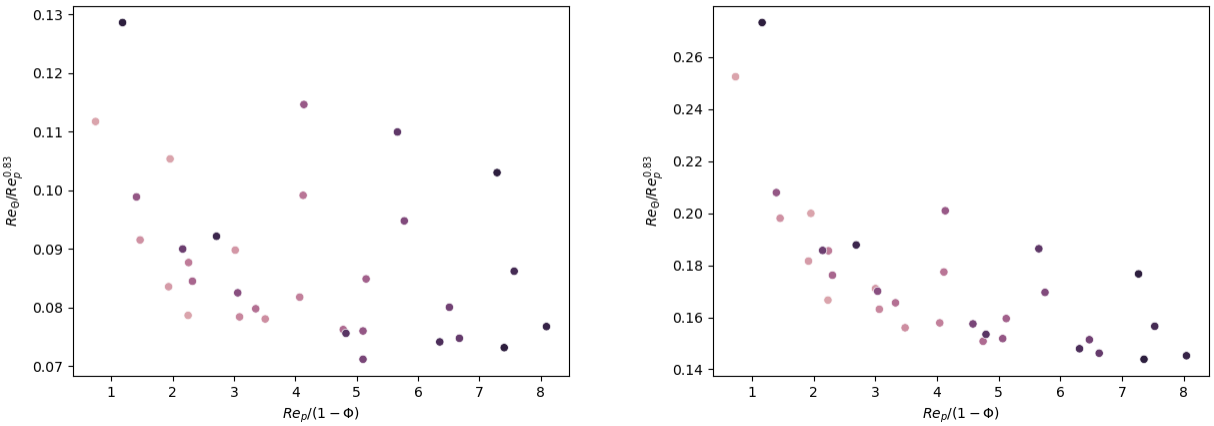


**Fig. 8. Ratio of $Re_\Theta$ to the primary influence of the adjusted Tang fit as a function of $Re_p/(1 - \phi)$, no filtering on the left and filtered, $\delta f = 8d_p$, on the right.**

Although these expressions fit the data quite well, we seek to improve the agreement through further refinement of the original model. Originally, we had hoped that the impact of Archimedes number would be an easy addition to improve model prediction. However, Fig. 6 shows significant spread in the data at very similar *Ar* values. This indicates that, while there could be some underlying *Ar*-dependence, it may be difficult to elucidate. This thought is confirmed in Fig. 7 where the primary fits, i.e., $Re_p^{0.83}$ and $Re_p^{0.73}$ for the unfiltered and filtered data, respectively, have been removed from $Re_\Theta$ and plotted against *Ar*. The lack of a strong correlation suggests that *Ar* has a weak influence on $\Theta$ or only as a secondary influence through other parameters.

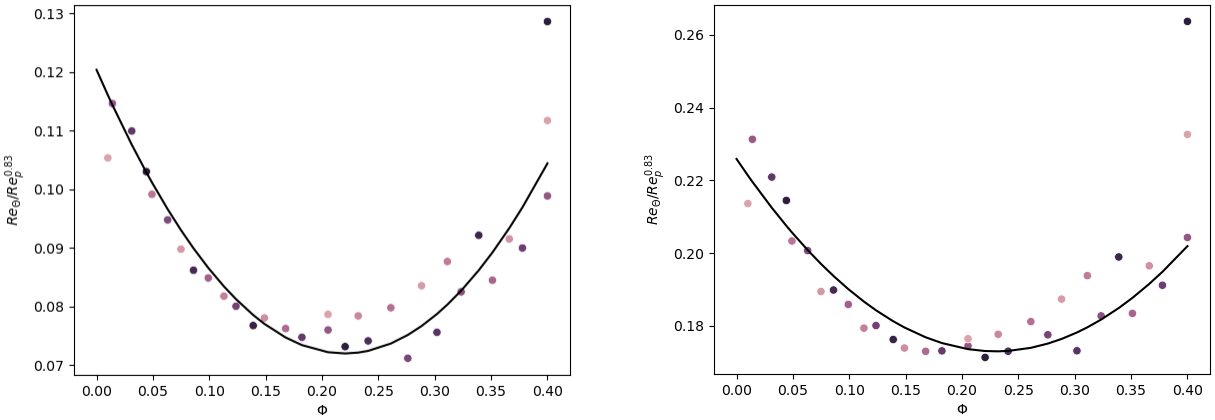


**Fig. 9. Ratio of $Re_\Theta$ to the primary influence of the adjusted Tang fit as a function of $\phi$, no filtering on the left and filtered, $\delta f = 8d_p$, on the right.**

To separate the effects of $\phi$ and $v_{slip}$, which are linearly combined in $Re_p$, the same quantity is plotted in Fig. 8 as a function of $Re_p$ / (1-$\phi$). Again, only a weak correlation is observed; i.e., the primary influence of $v_{slip}$ on $Re_\Theta$ (beyond $Re_p$ as already fit) is also weak. Conversely, Fig. 9 shows that there remains a significant influence of $\phi$ on $Re_\Theta$ beyond $Re_p$. As shown in Fig. 9, we fit a simple quadratic which takes the form $(\phi_0 - C_1 0.22)^2 + C_0 0.072$ with $C_1 = 0.22$ and $C_0 = 0.072$ for the unfiltered data and $C_1 = 0.23$ and $C_0 = 0.173$. The new expressions are given by,

$$Re_\Theta = ((\varphi_0 - 0.22)^2 + 0.072) Re_p^{0.83}\,, \tag{11}$$

for the unfiltered data, and

$$Re_\Theta = ((\varphi_0 - 0.23)^2 + 0.173) Re_p^{0.73}\,, \tag{12}$$

for the filtered data. Note that we have dropped the density ratio dependence and should be added back in with a leading coefficient of $1000^{1/2}$ for general modeling purposes.

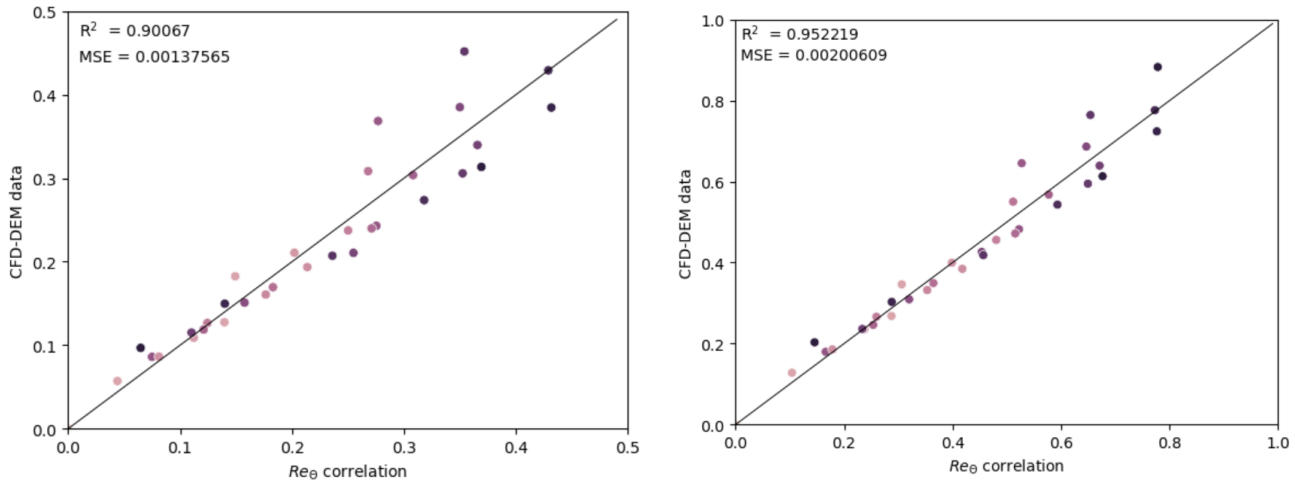


**Fig. 10. Parity plot comparison of the adjusted Tang model, Eqs. (9) and (10), to the time-averaged granular temperature, no filtering on the left and filtered, $\delta f = 8d_p$, on the right.**

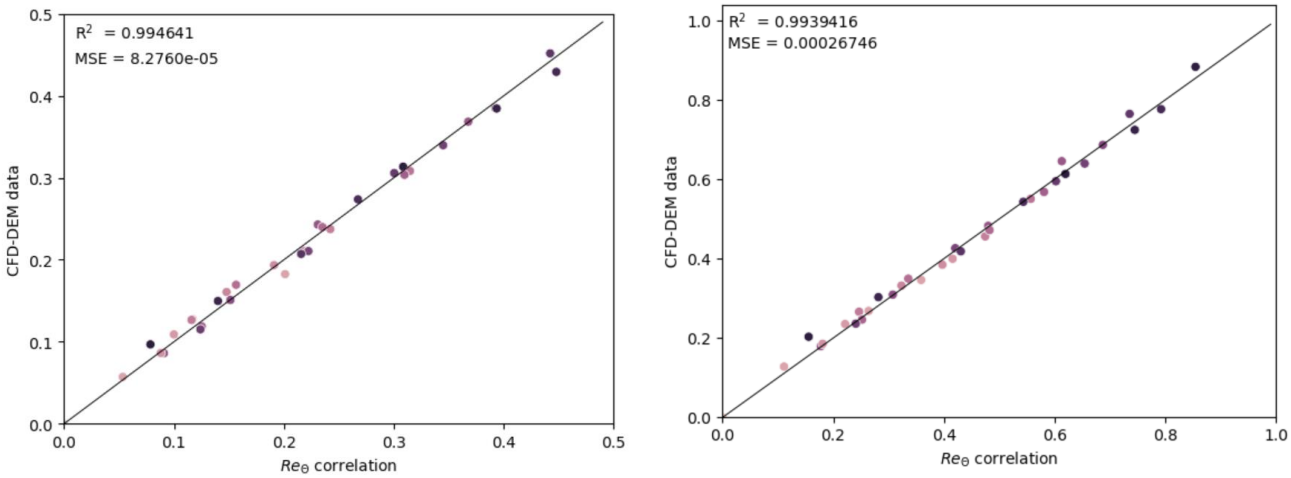


**Fig. 11. Parity plot comparison of the re-fit model, Eqs. (11) and (12), to the time-averaged granular temperature, no filtering on the left and filtered, $\delta f = 8d_p$, on the right.**

The models are compared to the raw data in Figs. 10 – 12. We refer to Eqs. (9) and (10) as the "adjusted Tang" model and Eqs. (11) and (12) as the "re-fit" model. Figures 10 and 11 show a marked improvement of the re-fit model over the adjusted Tang model. The $R^2$ values increase from 90% and 95% to over 99% for the unfiltered and filtered data, respectively. Additionally, the re-fit model is compared to the underlying time-dependent, phase-averaged granular temperature, i.e., the full 3300 dataset, in Fig. 12. Obviously, there is more noise comparing to 100x the amount of data, but the overall agreement is still very good, $R^2 > 0.97$ for both unfiltered and filtered data.

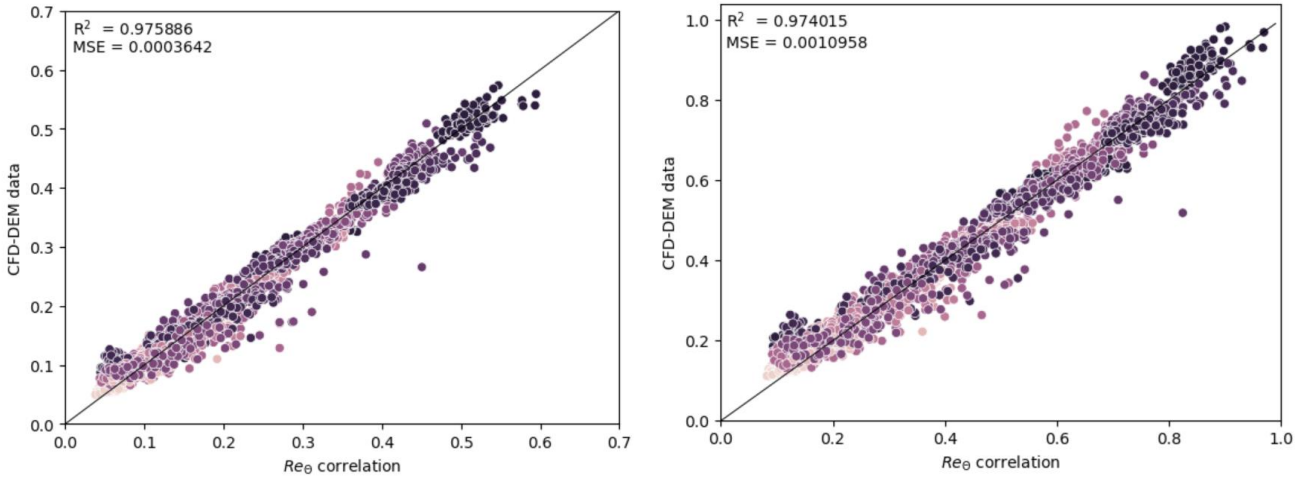


**Fig. 12. Parity plot comparison of the re-fit model, Eqs. (11) and (12), to the time-dependent granular temperature, no filtering on the left and filtered, $\delta_f = 8d_p$, on the right.**

## 3. CONCLUSIONS

In this study, we investigated methods to predict granular temperature. The data that was used for comparison and regression came from a large-scale CFD-DEM simulation campaign. The data is organized into 33 conditions, each with 100 data "snapshots" from a triply-periodic cluster-induced turbulence simulation. The CFD-DEM data was post-processed to provide phase- and (space) domain-averaged particle and fluid properties. Two types of post-processing were used: not filtering the particle data (beyond the native 8 fluid cell neighborhood deposition) and filtering with diffusion solve representing a Gaussian filter of width (at half max) $\delta_f = 8d_p$. Two models were used to predict the granular temperature: the homogeneous equilibrium reduction of the kinetic theory of Garzó et al. (2012) and the simple DNS-data fit of Tang et al. (2016). As expected, both models significantly under-predict the phase-averaged granular temperature from the CFD-DEM simulations. However, it was noticed that both models preformed reasonably, at least for the unfiltered data, when the actual (heterogeneous) slip velocity was used in the granular temperature expressions rather than the homogeneous value. Using this approach, we adjusted the Tang et al. (2016) correlation for both unfiltered and filtered data as given in Eqs. (9) and (10). The model was further improved by re-fitting a coefficient quadratic in concentration, $\phi$, given by Eqs. (11) and (12). The refit model compares favorably to not only the time-averaged data it was fit on but also to the full set of time-dependent data as shown in Fig. 12.

The two sets of post-processed data were independently, i.e., unfiltered *vs*. filtered, in this work. There is clearly a significant impact on the choice of post-processing filter on the data, specifically the granular temperature. Future work should focus on developing a more complete model as a function of the filter width. Additionally, the accuracy of the model is entirely dependent on accurately predicting the slip velocity which is known to be a very challenging issue in coarse representations of heterogeneous (clustered) particle-laden flows. Future work aimed at accurately predicting the heterogeneous (filtered) slip velocity based on the flow conditions would be of interest.

# REFERENCES

Agrawal, K., Loezos, P. N., Syamlal, M., & Sundaresan, S. (2001). The role of meso-scale structures in rapid gas–solid flows. *Journal of Fluid Mechanics*, **445**, 151-185.

Capecelatro, J., Desjardins, O., & Fox, R. O. (2016). Effect of domain size on fluid–particle statistics in homogeneous, gravity-driven, cluster-induced turbulence. *Journal of Fluids Engineering*, **138**(4), 041301.

Fullmer, W. D., & Hrenya, C. M. (2016). Quantitative assessment of fine-grid kinetic-theory-based predictions of mean-slip in unbounded fluidization. *AIChE Journal*, **62**(1), 11-17.

Fullmer, W. D., Liu, G., Yin, X., & Hrenya, C. M. (2017). Clustering instabilities in sedimenting fluid–solid systems: critical assessment of kinetic-theory-based predictions using direct numerical simulation data. *Journal of Fluid Mechanics*, **823**, 433-469.

Fullmer, W. D., & Hrenya, C. M. (2017). The clustering instability in rapid granular and gas-solid flows. *Annual Review of Fluid Mechanics*, **49**(1), 485-510.

Fullmer, W. D., & Hrenya, C. M. (2018). Continuum prediction of scale-dependent, anisotropic fluctuating kinetic energy in gas-solid flows. *Chemical Engineering Science*, **186**, 84-87.

Garzó, V., Tenneti, S., Subramaniam, S., & Hrenya, C. M. (2012). Enskog kinetic theory for monodisperse gas–solid flows. *Journal of Fluid Mechanics*, **712**, 129-168.

Igci, Y., Andrews IV, A. T., Sundaresan, S., Pannala, S., & O'Brien, T. (2008). Filtered two-fluid models for fluidized gas-particle suspensions. *AIChE Journal*, **54**(6), 1431-1448.

Igci, Y., & Sundaresan, S. (2011). Constitutive models for filtered two-fluid models of fluidized gas–particle flows. *Industrial & Engineering Chemistry Research*, **50**(23), 13190-13201.

Ozel, A., Gu, Y., Milioli, C. C., Kolehmainen, J., & Sundaresan, S. (2017). Towards filtered drag force model for non-cohesive and cohesive particle-gas flows. *Physics of Fluids*, **29**(10).

Radl, S., & Sundaresan, S. (2014). A drag model for filtered Euler–Lagrange simulations of clustered gas–particle suspensions. *Chemical Engineering Science*, **117**, 416-425.

Sarkar, A., Milioli, F. E., Ozarkar, S., Li, T., Sun, X., & Sundaresan, S. (2016). Filtered sub-grid constitutive models for fluidized gas-particle flows constructed from 3-D simulations. *Chemical Engineering Science*, **152**, 443-456.

Tang, Y., Peters, E. A. J. F., Kuipers, J. A. M., Kriebitzsch, S. H. L., & van der Hoef, M. A. (2015). A new drag correlation from fully resolved simulations of flow past monodisperse static arrays of spheres. *AIChE Journal*, **61**(2), 688-698.

Tang, Y., Peters, E. A. J. F., & Kuipers, J. A. M. (2016). Direct numerical simulations of dynamic gas-solid suspensions. *AIChE Journal*, **62**(6), 1958-1969.

# APPENDIX I

Another approach we took was to use a machine learning technique called multiple linear regression (MLR), using the particle, concentration, Archimedes number, and slip velocity as its features to predict the granular temperature. We hope to simply the equation to predict the granular temperature by finding a multiple linear equation which is easier to interpret. Using the LinearRegression and train_test_split functions in Python from scikit-learn library, we were able to create the models. After training and testing the models based each time-dependent data for each run, 3300 data points in total for each of the unfiltered and filtered datasets, we developed two multiple linear regression models. The MLR model for the unfiltered data is given by

$$\Theta \times 10^3 = 2.5389 v_{slip} - 8.3684\langle\phi\rangle + 0.040824 Ar\,, \tag{A1}$$

and the MLR model for the filtered data is given by:

$$\Theta \times 10^3 = 9.8774 v_{slip} - 22.0256\langle\phi\rangle + 0.10331 Ar\,. \tag{A2}$$

It was found that the MLR models were not as correlated with the data as the adjusted Tang model. The $R^2$ values for Eq. (A1) and (A2) are 0.77749 and 0.84442 on the unfiltered and filtered data, respectively. Therefore, we do no recommend using these fits.